Quantification of the cytoplasmic spaces of living cells with EGFP reveals arrestin-EGFP to be in disequilibrium in dark adapted rod photoreceptors

Jon A. Peet[1], Alvina Bragin[2], Peter D. Calvert[2], Sergei S. Nikonov[2], Shoba Mani[3,4], Xinyu Zhao[2], Joseph C. Besharse[5], Eric A. Pierce[2], Barry E. Knox[3,4] and Edward N. Pugh, Jr[2,*]

[1]Temple University School of Medicine, 3400 North Broad Street, Philadelphia, PA 19140, USA
[2]F. M. Kirby Center for Molecular Ophthalmology, University of Pennsylvania School of Medicine, Stellar-Chance Building, Room 309B, 422 Curie Boulevard, PA 19104-6069, USA
[3]Department of Biochemistry and Molecular Biology, and [4]Department of Ophthalmology, SUNY Upstate Medical University, 750 East Adams Street, Syracuse, NY 13210-2375, USA
[5]Department of Cell Biology, Neurobiology and Anatomy, Medical College of Wisconsin, 8701 Watertown Plank Road, Milwaukee, WI 53226-0509, USA
*Author for correspondence (e-mail: pugh@mail.med.upenn.edu)

Accepted 19 February 2004
Journal of Cell Science 117, 3049-3059 Published by The Company of Biologists 2004
doi:10.1242/jcs.01167

Summary

The hypothesis is tested that enhanced green fluorescent protein (EGFP) can be used to quantify the aqueous spaces of living cells, using as a model transgenic *Xenopus* rods. Consistent with the hypothesis, regions of rods having structures that exclude EGFP, such as the mitochondrial-rich ellipsoid and the outer segments, have highly reduced EGFP fluorescence. Over a 300-fold range of expression the average EGFP concentration in the outer segment was approximately half that in the most intensely fluorescent regions of the inner segment, in quantitative agreement with prior X-ray diffraction estimates of outer segment cytoplasmic volume. In contrast, the fluorescence of soluble arrestin-EGFP fusion protein in the dark adapted rod outer segment was approximately threefold lower than predicted by the EGFP distribution, establishing that the fusion protein is not equilibrated with the cytoplasm. Arrestin-EGFP mass was conserved during a large-scale, light-driven redistribution in which ~40% of the protein in the inner segment moved to the outer segment in less than 30 minutes.

Movies and supplemental data available online

Key words: Protein movement, Arrestin, Xenopus, Transgenesis

Introduction

Many cell functions depend on a polarized, non-equilibrium distribution of molecular constituents. Photoreceptors provide an excellent example in that both soluble and membrane-associated components of phototransduction function in a cellular compartment distinct from the site of macromolecular synthesis. The mechanisms that establish and maintain this polarity remain poorly defined, especially in the case of soluble proteins, but ultimately depend on a detailed understanding the cytoplasmic space through which macromolecules move. Efforts to characterize the cytoplasmic space with fluorescent molecular probes of various sizes have revealed a size-dependent partitioning into different subcellular regions (Janson et al., 1996; Luby-Phelps, 2000). The most likely explanation of this partitioning is 'sieving', i.e. the existence of compartments to which access depends on particle size. Quantification of the cytoplasmic space accessible to macromolecules of varying sizes is critical for defining the equilibrium distribution of a soluble macromolecule in a cell, thus providing a baseline against which nonequilibrium can be gauged.

A current problem involving the equilibrium distribution of soluble macromolecules is provided by the rod protein arrestin. Arrestin is an abundant soluble protein that plays an essential role in phototransduction by 'capping' phosphorylated rhodopsin (Wilden et al., 1986; Xu et al., 1997). Arrestin undergoes a large-scale redistribution from the inner segment (IS) to the outer segment (OS) in rods after light exposure (Broekhuyse et al., 1985; Broekhuyse et al., 1987; Philp et al., 1987; Whelan and McGinnis, 1988; Mendez et al., 2003; Peterson et al., 2003). But questions remain open about whether the initial distribution of arrestin in a dark adapted rod is determined by the relative water spaces of the compartments or by other factors such as specific binding, and to what degree active or passive processes govern its redistribution upon illumination.

To address such questions, we have used enhanced green fluorescent protein (EGFP) as a probe of the cytoplasmic space of living cells. Our experiments test the hypothesis that EGFP can serve as a quantitative measure of the cytoplasmic space. We quantify the expression of EGFP in living CHO cells and rod photoreceptors by using 3D laser scanning confocal microscopy. The distribution of EGFP in both cell types is consistent with the hypothesis that local EGFP fluorescence is proportional to the local aqueous volume fraction. We then examine transgenic *Xenopus* rods expressing an arrestin-EGFP fusion protein, and show that in the dark adapted state this soluble protein has a distribution highly distinct from that of

EGFP, and thus not in equilibrium with the cytoplasm. Finally we show that upon light-driven redistribution from the inner segment (IS) to the outer segment (OS), arrestin-EGFP obeys conservation of mass, rejecting the hypothesis that degradation and/or synthesis underlie the redistribution.

Materials and Methods

Description of the confocal laser scanning microscope and its calibration

We constructed a confocal laser scanning microscope (CLSM) based on the physical design and C++ image acquisition software of Hollingworth et al. (Hollingworth et al., 2001), using a TE300 inverted microscope (Nikon) fitted with a CFI_{60} (60×, 1.2 NA), water-immersion objective. The 3D point-spread function of the CLSM was measured with 0.1 μm diameter fluorescent microspheres. The normal scanning parameters were: *x-y* field size, 100 μm × 100 μm at 0.4 μm per pixel; *z*-step, 0.5 μm; voxel collection time 24 μs (cf. Suppl. data for details: http://jcs.biologists.org/supplemental/).

The relationship between the CLSM signal and EGFP concentration, [*EGFP*], was determined by scanning a 15 μl chamber loaded with solutions of recombinant protein (Cat. no. 8365-1 Clontech, Palo Alto, CA) whose concentration was determined with a spectrophotometer (λ20 UV/Vis, Perkin-Elmer), using published spectra and an extinction coefficient ε_{max}=55,000 cm^2 $mmol^{-1}$ at 488 nm (Tsien, 1998). This relationship between excitation intensity *I*, [*EGFP*] and fluorescence *F* was found to be described by a bilinear function of the two independent variables:

$$F = KI[EGFP] = KI_{max}\, 10^{-D}\, [EGFP], \quad (1)$$

where I_{max} is the maximum intensity, *D* the density of any filters in the excitation beam, and *K* a constant. Eqn 1 was inverted to estimate [*EGFP*] in living cells: thus, in the voxel at position (*x*, *y*, *z*)

$$[EGFP](x,y,z) = F(x,y,z) / (KI_{max}\, 10^{-D}). \quad (2)$$

Transgenic *Xenopus* and CHO cells: arrestin-EGFP fusion construct

The REMI method was used to create transgenic *Xenopus*, with EFGP and arrestin-EGFP (Arr-EGFP) fusion protein expression driven by the opsin promoter (Mani et al., 1999; Mani et al., 2001). CHO cells stably expressing EGFP were created with standard methods; the constructs are described in the supplemental data (Materials and Methods, Sections 2-5, http://jcs.biologists.org/supplemental/).

Quantitative western blotting and fluorimetry

For western blotting of CHO cells, the pellet of 1×10^6 cells was resuspended in 100 μl of non-denaturing lysis buffer (1% w/v Triton X-100; 50 mM TrisCl, pH=7.4, 300 mM NaCl, 5 mM EDTA, and protease inhibitor), kept on ice for 30 minutes, and spun at 21,000 ***g*** for 30 min at 4°C, and the supernatant collected. In control experiments to determine the maximum yield of protein, the resuspended material was sonicated 5× or subjected to freeze/thaw cycles. Western blotting of cell lysates was performed by running 10 μl of the supernatant on an SDS-PAGE gel calibrated with prestained molecular weight standards (Cat. no. 161-0372, BioRad), along with lanes containing 10 μl aliquots of rEGFP or rGFP (Clontech) whose concentrations were determined spectrophotometrically. An equivalent aliquot of supernatant of lysed non-expressing g1651a CHO cells was run as a control. After the initial electrophoresis, the gel contents were transferred electrophoretically to a nitrocellulose filter, blocked for 1 hour with 1% dry milk and exposed to EGFP antibody (Clontech, Cat. no. 8367 or Roche, Cat. no. 1814460) at 1/100 dilution in 1% dry milk PBS/Tween solution. The filter was then washed, exposed to a secondary antibody conjugated to alkaline phosphatase and washed again. Finally it was exposed to ECF substrate, fluorescence measured with a Storm phosphosphoimager and quantified with ImageQuant™ software (Molecular Dynamics).

The mass of EGFP in lysates of CHO cells was estimated fluorimetrically by scanning 20 μl aliquots with the CLSM, as was done with recombinant EGFP (Fig. S2, http://jcs.biologists.org/supplemental/). The total mass of protein was computed as the product of the concentration of EGFP multiplied by the lysate volume.

Recording chamber and basic protocol for living cells

The recording chamber was fabricated from plastic Petri dishes from whose center an ~3×3 mm cutout was milled; a number 1 coverslip was affixed to the bottom with wax, creating a volume of ca. 15 μl that could be readily searched. CHO cells passed into PBS or small pieces of dark-adapted *Xenopus* retina dissected under infrared illumination in oxygenated Ringer's solution (in mM: NaCl 111, KCl 2, $CaCl_2$ 1, $MgCl_2$ 1, $MgSO_4$ 0.5, NaH_2PO_4 0.5, HEPES 3, glucose 10, EDTA 0.01) were loaded into the chamber, after which it was sealed with a coverslip and vacuum grease. The experimental conditions were essentially those used in our laboratories for electrical recordings from amphibian photoreceptors. For the experiments with Arr-EGFP, all manipulations of the tissue, including the location of the cells to be scanned with the CLSM in the recording chamber, were performed with infrared light. Two steps were taken to avoid selection bias: (1) the chamber was initially viewed under infrared illumination and a piece of retina having the largest number of well oriented, contiguous rods selected; (2) in the offline data analysis, every intact rod scanned was processed.

Image segmentation and analysis of confocal data from cells

A user-driven interface was created with the Matlab programming language (Mathworks, Natick, MA) for the segmentation of CLSM data from CHO and rod cells (see supplemental data, Materials and Methods, Section 6, http://jcs.biologists.org/supplemental/). This '3D cookie cutter' allowed the 3D CLSM data of individual cells to be extracted from stacks of images and processed for further analysis. The concentration of EGFP in each voxel of a cell was determined with Eqn 2, and other statistics, including envelope cell dimensions and envelope volume, were computed. The total mass of EGFP in each cell was obtained by summing over the voxels defining the cell. A distinctive feature of the rod cell analysis was the derivation of a spline, measuring 1.6 μm in the *x*- and *y*- dimensions and 1 μm in the *z* dimension, along the central 'core' of each cell's 3D data.

Electron microscopy and immunohistochemistry

For EM, eyes from euthanized animals were fixed in 1.65% glutaraldehyde and 1% OsO_4 in phosphate buffer and embedded in epoxy resin as previously described (Pazour et al., 2002). For immunohistochemistry, eyes were placed in 4% paraformaldehyde in PBS at 4°C overnight, incubated overnight in 30% sucrose in PBS at 4°C, frozen in OCT and sectioned at 20 μm with a Leica CM 1850 cryostat. Sections were then blocked for 30 minutes and the primary antibody applied overnight at 4°C. The sections were then washed three times with PBS, and the secondary antibody applied for 1 hour. Primary antibodies and dilutions employed were against cytochrome *c* (1:250; Sigma, St Louis, MO), acetylated α-tubulin (1:1500; Sigma). Appropriate secondary antibodies conjugated to Cy3 (Jackson ImmunoResearch, West Grove, PA) and Alexa 555 (Molecular Probes, Eugene, OR) were used to complement EGFP fluorescence. After the final wash, sections were mounted with medium containing DAPI (Vectashield, Vector Laboratories, Burlingame, CA) and imaged with a Zeiss LSM-510 confocal microscope.

Results

Quantifying EGFP expression in CHO cells

Analysis with confocal laser scanning microscopy (CLSM)

To establish the accuracy of the CLSM for quantifying EGFP expression in living cells, we measured the fluorescence of a line of CHO cells (pDP3) that express EGFP, and compared the EGFP mass per cell estimated from CLSM data with the mass estimated by western blotting and fluorimetry. CHO cells were approximately spherical in shape, but varied in their volume and in their average fluorescence (Fig. 1). The average pDP3 cell volume determined with the CLSM was 1.17±0.54 pl (mean±s.d., n=485 cells). We determined the amount of EGFP in each voxel and summed the amounts over the cell volume to estimate the total mass of EGFP per cell. The average EGFP mass per cell was 6.9±0.8 attomols/cell (Table 1). A potential source of error is autofluorescence: however, the fluorescence intensity of control cells was more than 100-fold reduced from that of pDP3 cells (Fig. 1D), and so autofluorescence had negligible effect on the estimation of the EGFP concentration.

Quantitative western blotting and fluorimetry

Western blotting of pDP3 cell lysates yielded the estimate 5.1±1.8 attomols/cell, while fluorimetric analysis of aliquots of the same lysates yielded the estimate 5.4±1.1 attomols/cell (Fig. 2; Table 1). CHO cells not expressing EGFP gave no signal on western blots, but the autofluorescence of their lysate was measured and found to be more than 100-fold lower than the fluorescence of pDP3 cell lysate (Fig. 2). The western blotting and fluorimetry establish that the local fluorescence intensity of EGFP as measured with our photon-counting CLSM accurately reflects the local EGFP concentration, and can be used to derive quantitative estimates of the mass of EGFP in living cells.

Table 1. EGFP mass extracted from CHO (pDP3) cell data

Method	Mean±95% c.i. (attomols/cell)	Numbers (passaged 7 times):
Confocal fluorescence of live CHO cells	6.9±0.8	485 cells
Western blotting	5.1±1.8	14 blots
Lysate fluorimetry	5.4±1.1	7 lysates

The first column identifies the method of estimating the mass of EGFP per cell. The second column presents the results (one attomol=10^{-18} mol). The third column gives the numbers of cells (row 1; see Fig. 1), western blots (row 2) or fluorimetric assays (row 3; see Fig. 2) whose data were averaged. The data were collected from cells passaged seven different times over a period of 6 months.

The average concentration of EGFP in pDP3 cells estimated with analysis of the CLSM data was ~6 μM (6.9×10^{-18} mols/1.2×10^{-12} l), but ranged about 30-fold, from 0.7 to 20 μM over the population (Fig. 1C). This concentration variation provides grounds for testing the hypothesis that the distribution of EGFP reflects the local aqueous space of the cells.

EGFP equilibration hypothesis

EGFP is highly soluble and diffuses in cultured cells faster than any protein in its molecular weight class (Luby-Phelps, 2000). The rapid diffusion of EGFP in cells indicates that it interacts little with other cellular constituents, and suggests to us that it can serve as a marker for the local 'water fraction' of the cell. We formulate this idea as an hypothesis: 'EGFP is in equilibrium with the cell's cytoplasm'.

This hypothesis predicts that the ratio of the EGFP fluorescence intensity of a given volume element (voxel) to the maximal local fluorescence intensity of the cell

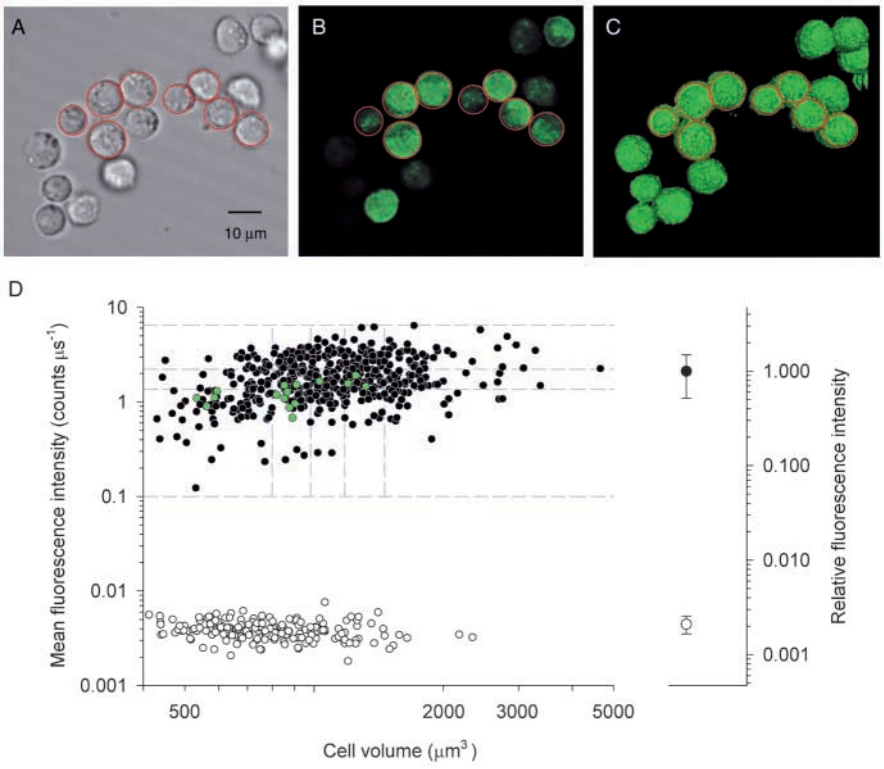

Fig. 1. Fluorescence intensity and volumes of CHO cells expressing EGFP. (A) Transmission image of pDP3 cells. (B) Fluorescence intensity of the cells in A, measured with the CLSM; this image is the average of two successive x-y scans taken at the z-level where the apparent cell diameters were maximal. (C) Three-dimensional surface renderings of the cells of panels A and B, from the viewpoint of the objective in the inverted microscope, and presenting for each cell an iso-intensity surface at a level ~3% of the maximum fluorescence. (D) Mean fluorescence intensity of 485 pDP3 cells (●) and 193 non-expressing control CHO cells (○), plotted as a function of the cell volume. The green filled symbols plot the data of the cells illustrated in panels A-C. The symbols to the right give the mean±s.d. of each population, scaled relative to the mean of the pDP3 cell fluorescence. The dashed lines show the boundaries of 15 bins into which the data were pooled to examine dependencies of the estimated aqueous volume fraction on cell volume and EGFP levels.

should provide an estimate of the voxel's fractional aqueous space: thus,

$$f_{\mathrm{aq,voxel}}(x,y,z) = \frac{F(x,y,z)}{F_{\max}}\ , \qquad (3)$$

where $f_{\mathrm{aq,voxel}}$ is the fraction of the voxel at location (x, y, z) to which EGFP has ready access, F is the fluorescence intensity, and $F_{\max}$ the maximum fluorescence. We estimated $f_{\mathrm{aq,\,cell}}$, the fraction of aqueous space of each cell, by calculating Eqn 3 for every voxel of the cell, and then averaging over the cell volume. The value of $F_{\max}$ was taken to be the average fluorescence intensity of the voxels of the cell comprising the upper Mth percentile of intensities, for M≥95%: the estimates were $f_{\mathrm{aq,cell}}$=0.53±0.06 for M=95% and $f_{\mathrm{aq,cell}}$=0.48±0.06 for M=99%. The value $f_{\mathrm{aq,cell}}$=0.54 is given in Alberts et al. [Table 12-2 (Alberts et al., 1994)] for hepatocytes. We tested for dependence of $f_{\mathrm{aq,cell}}$ on cell volume and expression level by partitioning the fluorescence data into 15 roughly equally populated bins defined by volume and average fluorescence intensity (Fig. 1D, dashed lines): there was no dependence of $f_{\mathrm{aq,cell}}$ on cell volume, but it is about 15% lower for cells in the lowest third of the distribution of intensities than for those in the highest.

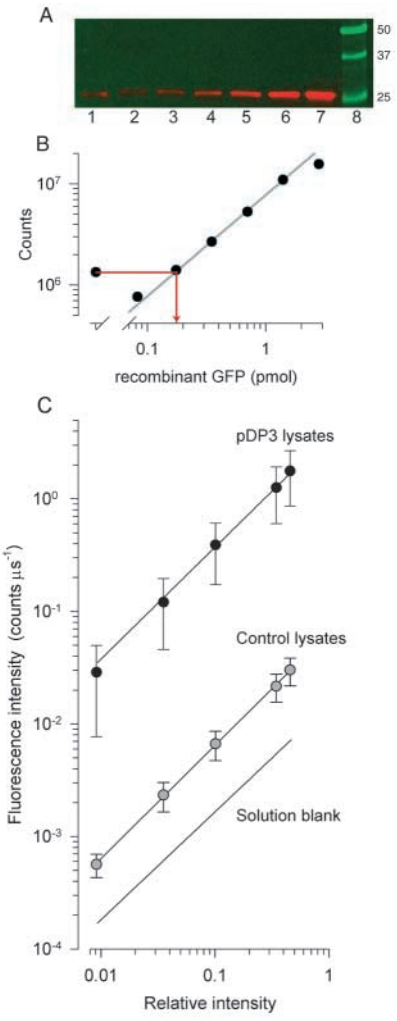

Fig. 2. (A) Quantitation of EGFP mass per CHO cell with western blotting and fluorimetry. Immunofluorescence of a gel stained with primary antibody against GFP. Lane 1 (red band) was injected with the lysate of 5×10^4 pDP3 cells, while lanes 2-7 contained incremented amounts of recombinant EGFP; lane 8 (green bands), molecular size calibration. (B) Fluorescence intensity of the bands of the gel in A as a function of loaded protein: each point corresponds to the intensity of the lane above it. The line is a least squares regression line fitted to the points in the linear range of the blot. The protein mass in the pDP3 lysate band (lane 1) is estimated from the projection of the band intensity (leftmost circle) onto the regression line, yielding for this experiment 0.2 pmols, or 4.0 amols per cell. (C) Fluorimetric analysis of cell lysates. Lysates of 10^6 pDP3 or non-expressing control cells in 100 µl of non-denaturing buffer were scanned in the CLSM in the same manner as recombinant EGFP (see Materials and Methods). Filled symbols show fluorescence (mean±s.d.) of lysates: ●, pDP3 cells (n=12 scans of 8 different lysates); ●, non-expressing cells (n=7 lysates). The unity slope regression line through the pDP3 lysate data corresponds to 57 nM recombinant EGFP, yielding 5.7 pmols total mass, or 5.7 amols/cell, in good correspondence with the value 5.4±1.1 amols/cell obtained from averaging estimates from regression analysis of the lysates of the 12 experiments.

Quantifying variation in the expression of EGFP among neighboring rods

Preliminary CLSM scans of isolated rods had fluorescence intensity distributions which appeared distinct from those of rods in intact pieces of retina, leading to the inference that separating rods from the retina initiated structural changes. Consequently, quantitative investigation required the use of small pieces of intact retina. In the intact retina rods are elongated, with several domains of distinctive structure and content and with neighbors exhibiting varying levels of EGFP fluorescence (Fig. 3), and so present several distinct challenges for quantifying expression.

Analysis of the spatial distribution of EGFP in individual rods

Using a '3D cookie cutting' method we analyzed the spatial distribution of EGFP in a population of rods (Figs 4, 6-8). The distribution of one rod excised from the scan data of Fig. 3B reveals several features of the EGFP distribution, including from left to right: the synaptic spherule, a brightly fluorescent nuclear and inner segment region, a dim segment tentatively identified as the ellipsoid by its position, followed by a relatively uniform outer segment whose distal tip is somewhat brighter (Fig. 4A). These features are quantified by plotting the fluorescence intensity distribution or profile along the 'core' of the cell (Fig. 4B, thickened red line), along with the profile distributions of seven other rods whose images were excised from the scan data of the same piece of retina (Fig. 3).

The EGFP equilibration hypothesis predicts that the profile distributions, when appropriately scaled, should be independent of the expression level. To test this we divided the fluorescence profile distribution of each rod by its maximum fluorescence intensity; these normalized profile distributions are plotted along with the average normalized profile of the 15 rods (Fig. 4C) scanned in the experiment shown in Fig. 3. The average profile of 57 rods scanned in 12 pieces of retina from 4 animals is very similar to that of the 15 rods from one piece of retina (Fig. 4D).

Features of the rod cytoplasm revealed by EGFP

Several distinctive features of the rod are highlighted by the EGFP profile distributions (Fig. 4). First, in each rod the most intense EGFP fluorescence is found in a broad region that surrounds and includes the nucleus. The apparently high aqueous volume fraction in this region is expected from many classic ultrastructural investigations, from experiments with small molecular weight fluorescent dyes (Olson and Pugh, 1993), and from the accessibility of the nucleus to EGFP

(Keminer and Peters, 1999; Moritz et al., 1999) (Fig. 5B). Second, each rod exhibits a sharp decrease in fluorescence intensity just to the left of the relatively flat profile along the OS (Fig. 4). This decrease can be unequivocally identified with the ellipsoid region of the rod which is densely packed with mitochondria, confirmed immunohistochemically with antibodies to cytochrome *c* (Fig. 5B) and by EM (Fig. 5E-G). The lowered EGFP fluorescence intensity in the ellipsoid region in living rods is qualitatively consistent with the EGFP equilibrium hypothesis, on the assumption that EGFP is excluded from the water space of the mitochondria. Third, every rod exhibits a bright fluorescent spot localized to the top and one side the ellipsoid (cf. Fig. 3B, red arrows; Fig. 5A, white arrows). Immunolabeling with an antibody against α-tubulin shows that this feature corresponds to the region of the basal body, where the cilium connecting the IS and OS originates (Fig. 5C,D). Histochemistry (Fig. 5B) and EMs (Fig. 5E-H) confirm that a space devoid of mitochondria is present there. Fourth, most rods exhibit a region of increased EGFP fluorescence that encompasses the tip of the outer segment (Fig. 4B,C). This latter feature is not so readily seen in the averaged profile distributions (Fig. 4D) as in the profiles of individual rods. The feature is diminished by averaging because the cell profiles were aligned at the junction of the IS and OS, but the OSs varied in the length. The third and fourth features revealed by EGFP have not been identified previously in ultrastructural studies in terms of increased aqueous volume fractions, and highlight the utility of EGFP for uncovering novel structural features of cells.

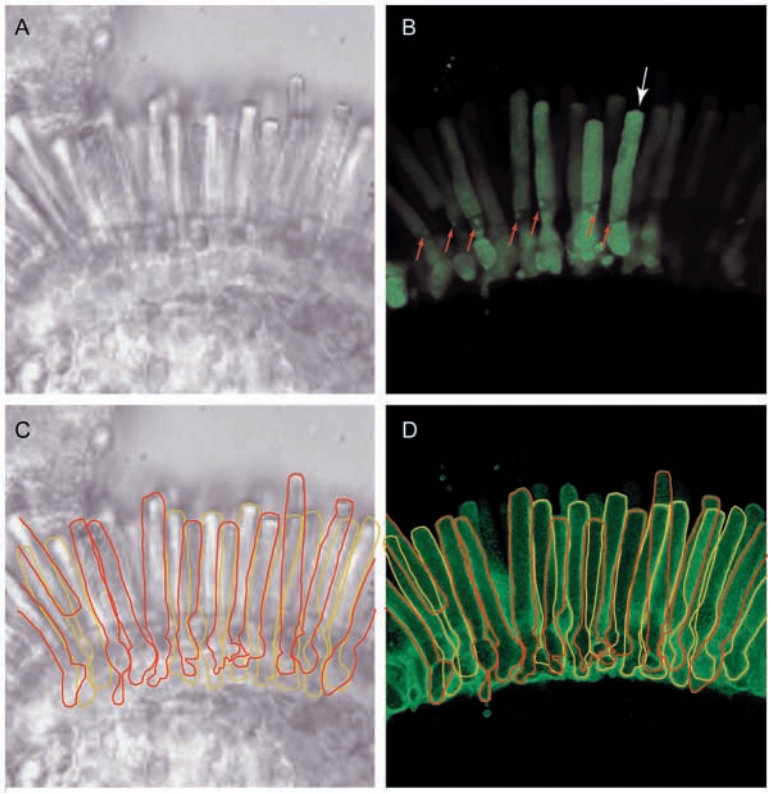

Fig. 3. Features of rod cells expressing EGFP. (A) Transmission image of a small piece of *Xenopus* retina in the recording chamber. (B) Three-dimensional rendering of CLSM scans of the piece of retina shown in A. The scan data are displayed using a linear gradient over the lower 50% of the fluorescence range to enhance visibility of weakly fluorescing rods. (The rod identified by the arrow in B is singled out for further analysis in Fig. 4A. The red arrows point to a small area of high fluorescence, a feature examined in Fig. 6.) (C,D) An outline of each rod identified in the 3D rendering was made: rods nearer the chamber floor have been outlined in red, while those further back in the stack have been outlined in yellow. In panel C these outlines have been superimposed on the transmission micrograph, illustrating the correspondence between the two images.

A quantitative test of the EGFP equilibration hypothesis

A quantitative prediction of the EGFP equilibration hypothesis can be derived from the ultrastructure of the rod determined from X-ray diffraction and neutron scattering by living rods (Table 2). Such data reveal that rod discs, which are closed to the cytoplasm (Chen et al., 2002), occupy about 50% of the envelope volume in the 'core' of the OS. Thus, the hypothesis predicts that fluorescence in the OS core should be about 50% of the maximal fluorescence in the rod. This prediction is borne out by the average, normalized profiles: along the OS the normalized profiles are very near 50% (Fig. 4C,D). This prediction is further examined in Fig. 6, whose upper panel plots the apparent concentration of EGFP along the OS core as a function of the maximal concentration of EGFP in the IS: the hypothesis predicts that the points should fall on a line of slope ~$\frac{1}{2}$. For the population of 57 rods, the ratio of outer segment core EGFP concentration to the maximal IS concentration was 0.51±0.04 (mean±95% confidence intervals). Thus, over an ~300-fold concentration range differential EGFP binding is not distorting the profiles.

Table 2. Estimates of the cytoplasmic volume fraction of the rod outer segment (OS)

Method	Resolution (Å)	Preparation	OS volume (fraction)	References
X-ray diffraction	8	Intact untreated retinas	0.49	Worthington, 1974
X-ray diffraction	25	Magnetically oriented rods	0.51	Schwartz et al., 1975
Neutron scattering	75	Retinas at 5°C	0.53	Yeager, 1976
Birefringence with imbibition	NA	Isolated rod outer segments	0.45-0.55*	Corless and Kaplan, 1979

Low angle X-ray and neutron diffraction studies were performed with frog (*Rana* sp.) retina or rod outer segments freshly prepared in Ringer's solution. Each study produced an electron or nucleon density profile of the repeat unit of the rod outer segment, in each case found to be 295-300 Å. The fraction of water space in the outer segment was computed as the distance between the disc faces in the repeat unit.

*Results from analysis of a 3-dielectric model analysis applied to the birefringence gradient of freshly prepared frog rods.

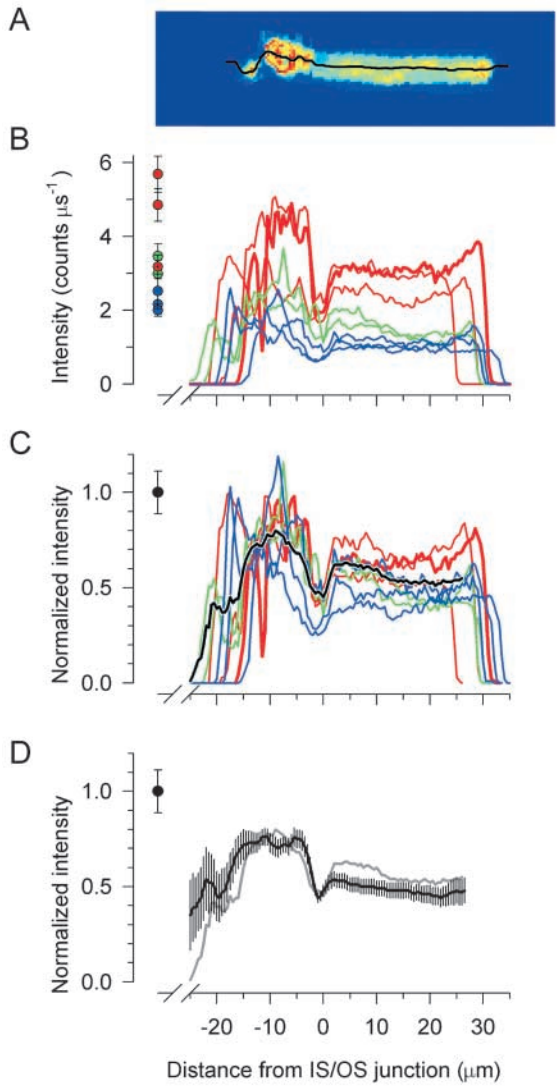

Fig. 4. Quantification of the spatial distribution of EGFP in living *Xenopus* rods. (A) EGFP distribution in a single rod. The voxels corresponding to the rod identified in Fig. 3B (white arrow) were excised from the stack of 2D CLSM scans, and projected onto a plane parallel to the OS axis: the panel is a false-color representation of the fluorescence distribution in the average of three scans spanning a thickness of 1.5 μm. The black line through the image is the automatically determined 'z-spline' path through the cell's core along which a fluorescence intensity profile was computed. (B) Fluorescence intensity profiles of 8 rods from the piece of retina illustrated in Fig. 3, segregated with colors to indicate different levels of fluorescence: red for most intense, green for mid-level and blue for least intense (the profile of the rod of panel A is identified with a thickened red line). Panels A and B are aligned on the abscissa, and the profiles of all rods have been aligned at the junction between the IS and OS (x=0). The colored symbols at the left give the mean (±s.d.) fluorescence of the voxels of the entire IS of each rod having the top 5th percentile of intensities (comprising, on average, 460 voxels per rod). In the OS region the spline goes through the center or 'core' of the rod discs, whereas in the IS the spline randomly encounters high and low fluorescence voxels. (C) The profile distribution of each rod in panel B has been normalized by the value of the corresponding colored circle plotted at the left of the graph. The thickened black line plots the average of the normalized intensity profiles of the 15 rods 'cut' from the piece of retina illustrated in Fig. 3. The black symbol to the left represents the normalization value (unity), and the error bar gives the average coefficient of variation (s.d./mean) of the top 5th percentile of voxels of the inner segments of the 15 rods. (D) Grand average normalized intensity distributions of rods expressing EGFP. Data such as shown in panel C were pooled from 57 rods whose profiles were extracted from CLSM scans of 11 pieces of retina from 5 *Xenopus* tadpoles and froglets ranging from 4 weeks to 9 months of age. Error bars are 95% confidence intervals. (The average trace from panel C is shown in light gray for comparison.)

Arrestin-EGFP is not in equilibrium with the cytoplasm in dark adapted rods

Many important applications of EGFP arise from its capacity to serve in fusion proteins as a reporter for the locations and movements of proteins in cells. We took advantage of this capacity by examining the distribution of an arrestin-EGFP fusion protein (Arr-EGFP) expressed in rods under the *Xenopus* opsin promoter. In the dark-adapted state, Arr-EGFP is distributed differently from EGFP (Fig. 7A): first, the OS has less than 40% of the Arr-EGFP expected were the protein distributed freely (Fig. 7B,C); second, Arr-EGFP is concentrated in the region of the IS adjacent to the ellipsoid, and largely excluded from a broad region around the nucleus accessible to EGFP. Displays of the most intensely fluorescent voxels reveal the high concentration of Arr-EGFP just below and in a small pocket to one side of the ellipsoid (Fig. 7D).

Quantitative assessment of the light-induced redistribution of arrestin-EGFP

Bleaching of rhodopsin is thought to alter the distribution of arrestin by partitioning much of the soluble fraction onto the disc membranes of the outer segment, where rhodopsin resides (Mangini and Pepperberg, 1988; Mangini et al., 1994; Peterson et al., 2003). However, the immunocytochemical tools used to assess the apparent movement in some experiments have not permitted a quantitative evaluation of arrestin partitioning, and all or a portion of the apparent redistribution could reflect epitope masking as hypothesized to explain the light-dependent redistribution of transducin (Roof and Heth, 1988), and/or turnover of the protein (Azarian et al., 1995). We assessed the redistribution of Arr-EGFP in individual rods quantitatively after exposure of pieces of isolated retina to light that bleached all the rhodopsin (Fig. 8). By 30 minutes after the exposure, 40% of the Arr-EGFP initially in the IS had moved to the OS. This resulted in an almost twofold increase in the Arr-EGFP mass in the OS (Fig. 8B,C), including an increase at the very tip and a banding pattern, previously reported (Peterson et al., 2003). By 1 hour the Arr-EGFP distribution was reverting to its initial state. We derived the total mass of Arr-EGFP in each rod, integrating the fluorescence over the IS and OS, and comparing the sums in light and in darkness. Because conservation of mass is obeyed (Fig. 8C), we conclude that relocation of portions of an existing pool of Arr-EGFP in the IS, rather than protein synthesis or degradation, account for the redistributions in the hour following light exposure.

Our data may underestimate the full magnitude of the Arr-EGFP transfer in vivo. In a few rods more than 80% of the total

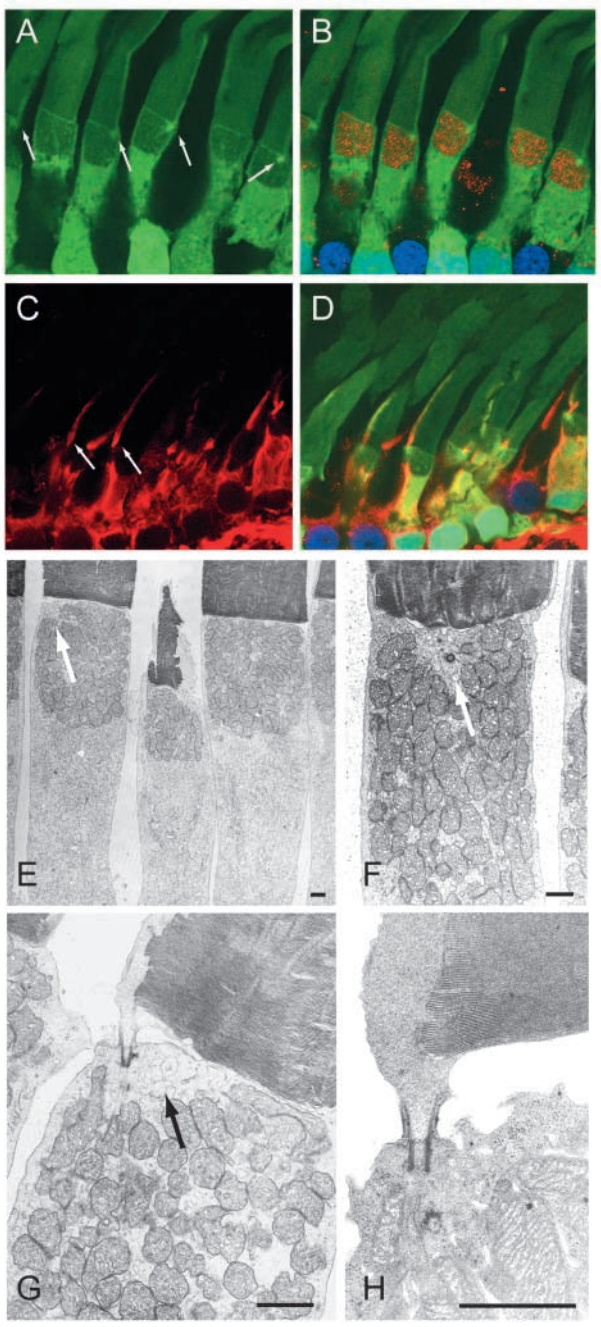

Fig. 5. *Xenopus* rod aqueous spaces revealed by EGFP and confirmed by immunohistochemical labeling of cytochrome *c* and α-tubulin, and by EM. (A) Confocal image of transverse frozen section of retina with only the EGFP channel activated. Arrows point to bright dots that localize just below the OS, which align with a green line that projects up the OS. (B) Same section as in A, showing immunostaining of cytochrome *c* (red) and the nucleus with DAPI (blue). The green fluorescence in the same location as the DAPI labeling shows EGFP to be present in the nucleus. Note the presence of three cone nuclei (deep blue) which show no green labeling; these cones give rise to dark regions in the images of A and B. (C) Confocal image of transverse frozen section labeled with antibody against acetylated α-tubulin (red), which identifies the cilium and axonemes of two rods (arrows) and two cones (no arrows). (D) Same image as in C, but with the EGFP channel activated: the bright green dots are seen to localize at the projection of the axoneme to the top of the ellipsoid region. The EGFP channel is relatively less intense than in A and B because some of the protein is lost owing to the use of Triton to enable the antibody access to α-tubulin (Kaplan et al., 1987). When *z*-stacks of such confocal images are scanned, every single rod shows the features illustrated in these panels. (E-H) Montage of EM images of the ellipsoid and basal disc region of *Xenopus* rods: in these panels one can see a region devoid of mitochondria immediately surrounding the basal body of the cilium (arrows). Scale bars, 1 μm.

Arr-EGFP was found to be initially in the IS, and up to 90% was found in the OS 30 minutes after bleaching. Exposure to the fluorescence excitation beam necessarily bleaches rhodopsin, and only cells closest to the floor of the chamber of the inverted microscope are in the fully dark adapted state when their confocal imaging commences.

Discussion

The investigations reported here focus on the *EGFP* equilibration hypothesis, an hypothesis with broad implications for cell biology. We have tested this hypothesis quantitatively, shown it to be generative in producing novel insights into cell structure, and used it to reject the hypothesis that arrestin, a major soluble protein of phototransduction, is in equilibrium with the cytoplasm of dark-adapted rod cells, as we now discuss.

The cytoplasm as a 'molecular sieve' and EGFP as a probe for aqueous spaces of living cells

The cytoplasm behaves as a 'molecular sieve', so that molecules of different sizes have differing degrees of access to subcellular cytoplasmic spaces (Luby-Phelps, 2000). There is thus a need for macromolecular probes of the cytoplasm. The properties of EGFP make it an ideal probe for aqueous spaces and more specifically for the cytoplasm, as formalized in the EGFP equilibration hypothesis (see above section 'EGFP equilibration hypothesis'). These properties include its high extinction coefficient (ε_{max}=55,000 cm^2 $mmol^{-1}$) and fluorescence quantum efficiency (γ~0.7), its low photodestruction rate (~10^{-7}) and its exceptionally high mobility in cells (D/D_o~0.5) (Tsien, 1998; Luby-Phelps, 2000). The high mobility of EGFP in cells indicates that EGFP undergoes little or no binding interactions, and thus will equilibrate with the cytoplasm and communicating aqueous spaces rapidly. Our results showing that the ratio of fluorescence intensity of EGFP in the rod OS relative to the maximal fluorescence of the IS is independent of absolute level of expression, support the absence of specific binding interactions over the concentration range from 3 to 300 μM (Fig. 6).

The EGFP equilibration hypothesis passes qualitative and quantitative tests

Several features of the distribution of EGFP in rods are qualitatively consistent with the EGFP equilibration hypothesis. The ellipsoid region of the rod, which is packed with mitochondria (Fig. 5B,E-H), has lower EGFP fluorescence than neighboring regions of the IS and OS (Fig.

3B, Fig. 4B,C, Fig. 5A). The OS, whose volume is substantially occupied by disc membranes, also has reduced fluorescence (Fig. 3B, Fig. 4B, Fig. 5A). In contrast, the region of the IS around the nucleus and the synaptic spherule, which have relatively high cytoplasmic content, have relatively high EGFP fluorescence.

Rod ultrastructure provides a rigorous basis for a quantitative test of the EGFP equilibration hypothesis. Investigations of intact amphibian rods with X-ray diffraction, neutron diffraction and birefringence measurements have produced estimates of the cytoplasmic volume fraction of the OS core of ~0.5 (Table 2). When these estimates are combined with the EGFP equilibration hypothesis, it is predicted that EGFP fluorescence in the core of the OS should be about 50% that of the most intensely fluorescing voxels of the IS. This prediction was confirmed and shown to be independent of expression level over a large concentration range (Figs 4, 6).

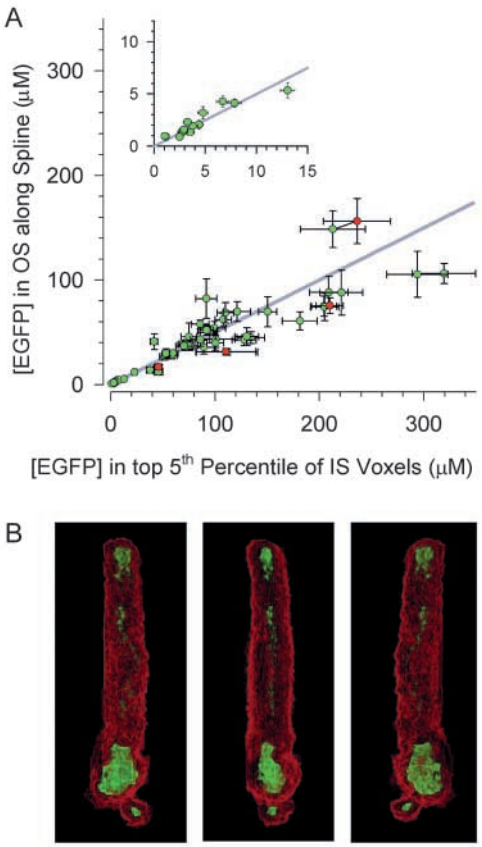

Fig. 6. Quantitative test of the EGFP equilibration hypothesis in *Xenopus* rod cells. (A) Each point gives the average concentration of EGFP in a rod OS derived from a profile analysis such as illustrated in Fig. 5A,B, plotted as a function of the maximal concentration of EGFP in the rod IS. The gray lines have a slope of $\frac{1}{2}$ and plot the prediction of the EGFP equilibration hypothesis that the OS should exhibit 50% of the fluorescence intensity of the brightest voxels of the IS. The inset shows the distribution in the lowest corner of the main plot, i.e. the initial 15 μM of the abscissa on an expanded scale. The red circles plot scan data of cells after a complete bleaching exposure; pre-bleach scans of the same cells were unchanged. (B) Display of the brightest 5% of the voxels (green) and the dimmest 5% (red) of the rod identified by the arrow in Fig. 3B; three orientations of the rod are provided. Autofluorescence levels of control rods were comparable with those of CHO cells (Fig. 1D) under our experimental conditions, and thus negligible in comparison with cells having average [EGFP] in the micromolar range.

EGFP reveals novel features of the rod cytoplasm: the vestibule and the cytoplasmic cap

The distribution of EGFP in rod cells has revealed novel features of potential importance to the distribution of soluble

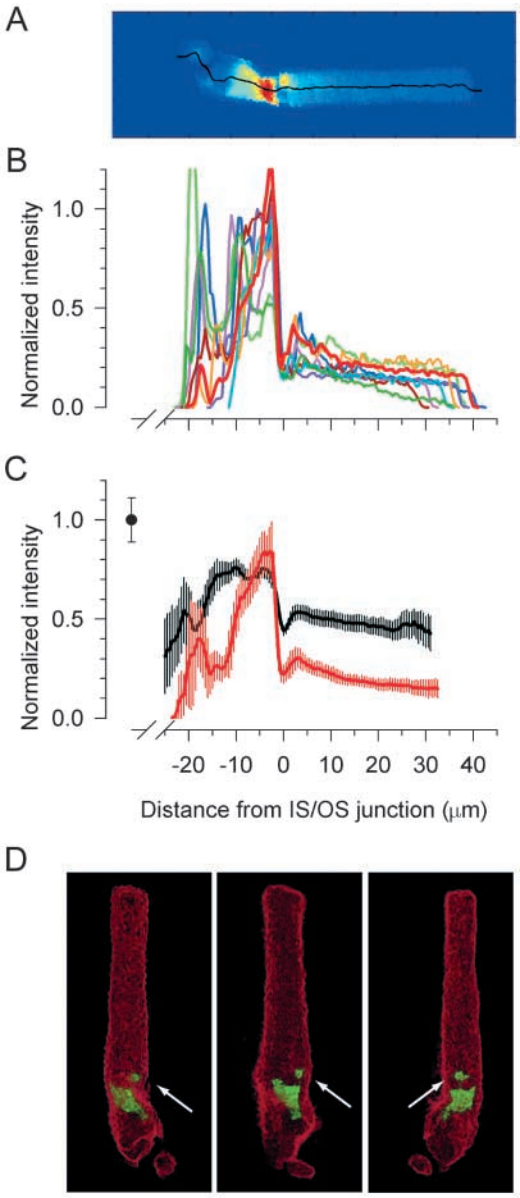

Fig. 7. Distribution of Arr-EGFP in dark adapted rods. (A) Pseudocolor representation of the distribution of Arr-EGFP in a dark-adapted rod. (B) Profile distributions along splines of the rod of panel A (thickened red trace), along with those of nine other rods from the same piece of retina, scaled by the intensity of the voxels of the inner segment having the top 5% fluorescence intensity. (C) Average fluorescence distributions (red trace) of Arr-EGFP in 15 rods from two animals compared with the average distribution of EGFP (black trace; cf. Fig. 4D); error bars are 95% confidence intervals. (D) Three-D rendering of the rod in A in which the dimmest 5% of the voxels are shown in red, whereas the 5% most intensely fluorescing voxels are shown in green.

proteins. One of these is the bright dot region localized to the ellipsoid immediately below the connecting cilium (Figs 3, 5). The EGFP equilibration hypothesis provides the basis for interpreting this spot as a region of increased water space available to soluble proteins immediately proximal to the connecting cilium, so we propose to name this space the 'vestibule' to the connecting cilium and OS. These results draw attention to the role of the connecting cilium as a cytoplasmic conduit to the OS (Pulvermuller et al., 2002).

Another novel feature revealed by EGFP corresponds to an increase in fluorescence near the tip of the OS (Fig. 4, Fig. 6B). Prior work has demonstrated changes in the uptake of fluorescent probes (Matsumoto and Besharse, 1985) and in ultrastucture (Matsumoto et al., 1987) at the distal tip of *Xenopus* rods associated with the onset of disc shedding and phagocytosis. The EGFP equilibration hypothesis allows these changes to be interpreted as an increase in cytoplasmic space accompanying the preparation of the tip of the OS for phagocytosis. We propose to call this newly defined structure the 'cytoplasmic cap' of the OS. An important structural correlation is that the rod axoneme has been found to terminate at about 2/3 the length of the OS (Kaplan et al., 1987), close to the position where the increase in cytoplasmic content begins (Fig. 4B,C).

Arrestin-EGFP disequilibrium in dark adapted rods

Arrestin is a soluble protein that binds phosphorylated rhodopsin, greatly reducing the latter's ability to activate the G-protein transducin in the visual cascade (Wilden et al., 1986; Xu et al., 1997). Our results establish definitively that Arr-EGFP is not in equilibrium with the cytoplasm of dark adapted rods (Fig. 7), and thus predict the existence of a mechanism that produces and maintains a disequilibrium in the dark adapted state. Since a large fraction of the Arr-EGFP in the IS can move rapidly to the OS when rhodopsin is bleached (Fig. 8), the mechanism that establishes the disequilibrium must be quickly reversible. Two plausible and non-exclusive hypotheses about the nature of the mechanism are these: (1) a signal-modulated 'gate' near or in the connecting cilium; and (2) binding sites in the rod IS with strong, but lower effective affinity for arrestin than bleached and/or phosphorylated rhodopsin. A specific version of hypothesis 1 has been proposed (Pulvermuller et al., 2002), which provides evidence that the calcium-binding protein centrin-1 locates to the connecting cilium, and binds the visual transduction protein, $G_t\alpha$. One way that a centrin-1-based mechanism might work is through a signal-dependent change in 'sieving': thus, complex formation by proteins in the dark-adapted state could create a 'sieve' in the connecting cilium that would only permit molecules of a certain size to transit. Our results suggest that EGFP is able to pass the most restrictive state of the sieve or gate, since the distribution of EGFP in the IS and OS in

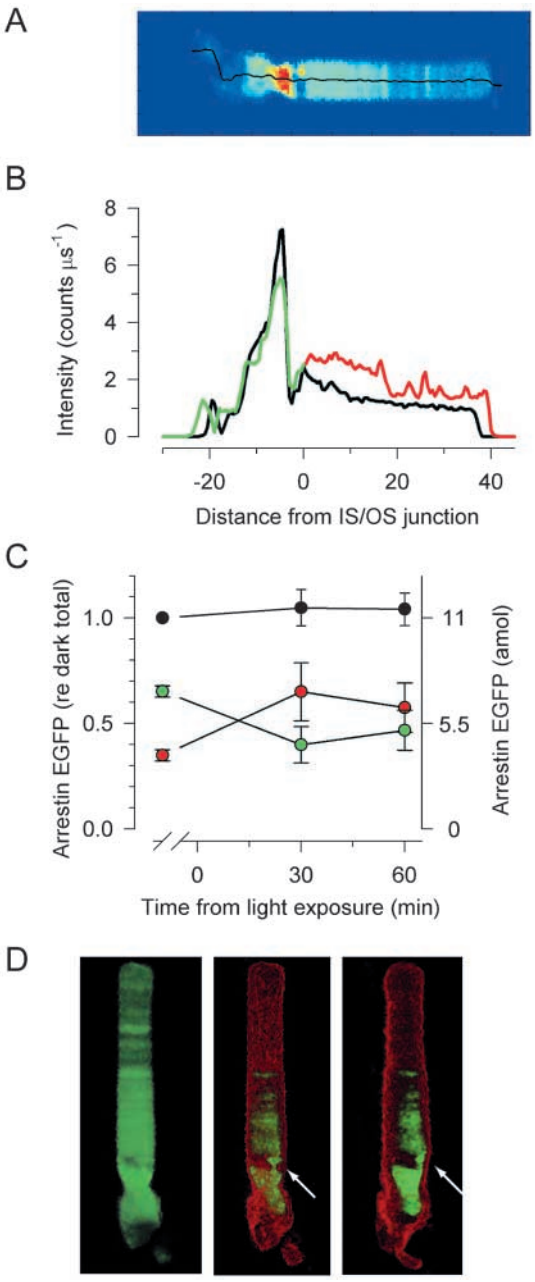

Fig. 8. Redistribution of Arr-EGFP fusion protein upon exposure of the retina to light and test of conservation of total protein. (A) Pseudocolor representation of the fluorescence intensity of a *Xenopus* rod expressing the fusion protein, Arr-EGFP 30 minutes after a 30 second light exposure that bleached all the rhodopsin; the dark adapted profile of the same rod is shown in Fig. 8A. (B) Intensity distributions along the rod in the dark (black) and 30 minutes (green for the IS; red for the OS) after the bleaching exposure. (C) Test of the hypothesis that total Arr-EGFP in the rod is conserved before and after the bleaching exposure. The mass of Arr-EGFP in the OS (red circles) and in the IS (green circles) was determined in the dark, and at 30 and 60 minutes after the bleaching exposure, and the sum (black circles) computed. For 10 rods from four separate pieces of retina, the same analysis was followed, and the data of each rod was normalized by the total Arr-EGFP in the cell in the dark (left axis). The scale on the right gives the Arr-EGFP mass for the average cell of the population; individual rods had up to 30 amols. Error bars are 95% confidence intervals. Conservation of Arr-EGFP is represented by the fact that the total (black circles) remains constant over the ca. 1.5 hour experiment. (D) 3D renderings of the distribution of Arr-EGFP of panel A at 30 minutes after the bleaching exposure: the leftmost images displays the fluorescence in a linear gradient; the middle and rightmost images show the brightest 5% voxels (green), and the dimmest 5% (red), in two orientations of the rod.

individual rods scanned with the CLSM when initially dark adapted, and re-scanned after they are fully bleached cells, is not materially different (Fig. 6).

In its simplest form, hypothesis 2 would specify that the apparent non-equilibrium distribution of arrestin-EGFP in the dark-adapted state reflects a differential binding in the IS and OS compartments. Thus, in the dark-adapted rod there would be a substantial population of arrestin binding sites in the IS combined with relatively few binding sites in the OS; bleaching of rhodopsin (whose concentration in the OS, in relation to the cytoplasm, is 6 mM) would then create a large population of binding sites, and arrestin would redistribute passively, as the soluble fraction in the OS partitions onto the disc membranes, in which the GPCR rhodopsin resides as an integral membrane protein. Mendez et al. have shown that light-dependent arrestin redistribution occurs in the absence of phosphorylation by the GPCR kinase GRK1 (Mendez et al., 2003). Their results reject the specific form of hypothesis 2 that identifies the light-dependent binding sites to be phosphorylated rhodopsin and, if the hypothesis is to be rescued, require the existence of light-dependent binding in the OS that is not dependent on phosphorylation by GRK1. Owing to the enormous concentration of rhodopsin in the OS, the hypothesis could remain viable if bleached but unphosphorylated opsin has weak affinity for arrestin, or if other binding sites such as membrane phosphoinositides are regulated by light, as has been shown for *Drosophila* photoreceptors (Lee et al., 2003).

Conservation of protein mass make it unlikely that de novo synthesis and/or degradation underlies the redistribution of arrestin-EGFP

The redistribution of arrestin upon strong bleaching of the rods of amphibia and mammals has been reported by many investigators (Broekhuyse et al., 1985; Broekhuyse et al., 1987; Philp et al., 1987; Mangini and Pepperberg, 1988; Whelan and McGinnis, 1988; Peterson et al., 2003; Mendez et al., 2003). Our results with Arr-EGFP show that this redistribution can be quantified in living rods in culture, opening the door to novel manipulations of mechanisms that might govern or affect the redistribution. Conservation of protein mass is obeyed over an hour period during the redistribution of Arr-EGFP to the OS, and redistribution of some of the protein back to the IS (Fig. 8C). This observation makes it unlikely that de novo synthesis and/or degradation contribute to the redistribution. Ongoing experiments are addressing the detailed time course and bleaching dependence of the redistribution. Knowledge of the cytoplasmic spaces of the rod will be critical to testing the hypothesis that arrestin redistribution is passive.

Problems for and further tests of the EGFP equilibration hypothesis

Critical to the estimation of the cytoplasmic volume fraction with EGFP is a satisfactory estimate of F_{max}, which sets the scale for conversion of fluorescence intensity (Eqn 1; Fig. 4B,C). We used the average fluorescence of the voxels having intensities at and above the 95th percentile to estimate F_{max}. This choice was based on the desire to have a statistically reliable sample and, for typical rods and CHO cells, 400 to 500 voxels were above the 95th percentile cuton. However, a 99th percentile criterion leads to ~10% lower aqueous volume fraction estimate in pDP3 cells, and an approximately 5% lower estimate of that of the outer segment. These observations call for caution and further investigation of the intrinsic and experimental factors affecting estimation of F_{max}.

Another problem for the EGFP equilibration hypothesis is that EGFP has access to the nucleoplasm (Keminer and Peters, 1999; Moritz et al., 1999) (Fig. 4, Fig. 5A,B). While such access does not per se exclude equilibration with the cytoplasm, it places additional constraints and could under some conditions perturb the equilibrium distribution, and calls attention to a key assumption of the hypothesis, namely that EGFP is distributed rapidly in a cell relative to any transients in translation and/or proteolysis. We have observed no measurable changes in the distribution of EGFP in single rod cells over periods exceeding 1.5 hours, including periods before and after exposure to light that completely bleaches all the rhodopsin (Fig. 6A). Calculations based on the time for small fluorescent probes to reach equilibrium in rods in which diffusion is greatly hindered (Olson and Pugh, 1993) suggest that equilibration with a step source of EGFP in the inner segment should take no more than tens of minutes in rods. Thus, given a half-life ~1 day (Verkhusha et al., 2003) one would expect the distribution of EGFP to be equilibrated in small cells. Nonetheless, it will be important to measure the time course of equilibration of EGFP and other GFP variants from point sources, and quantify the stability of the apparent equilibrium distribution – experiments we are actively pursuing.

This work was supported by the Research to Prevent Blindness Foundation (grants NIH EY02660, EY12975, EY12910) and the Human Frontiers of Science Program. We thank J. K. Blasie for helpful discussion of rod X-ray diffraction data and V. Y. Arshavsky for valuable comments. We are grateful to F. Letterio, J. Andrews-Labenski, E. L. Lu and R. Weldon for valuable assistance.

References

Alberts, B., Bray, D., Lewis, J., Raff, M., Roberts, K. and Watson, J. D. (1994). *Molecular Biology of the Cell*, 3rd edn. New York, NY: Garland Science.

Azarian, S. M., King, A. J., Hallett, M. A. and Williams, D. S. (1995). Selective proteolysis of arrestin by calpain. Molecular characteristics and its effect on rhodopsin dephosphorylation. *J. Biol. Chem*. **270**, 24375-24384.

Broekhuyse, R. M., Tolhuizen, E. F., Janssen, A. P. and Winkens, H. J. (1985). Light induced shift and binding of S-antigen in retinal rods. *Curr. Eye Res.* **4**, 613-618.

Broekhuyse, R. M., Janssen, A. P. and Tolhuizen, E. F. (1987). Effect of light-adaptation on the binding of 48-kDa protein (S-antigen) to photoreceptor cell membranes. *Curr. Eye Res.* **6**, 607-610.

Chen, C., Jiang, Y. and Koutalos, Y. (2002). Dynamic behavior of rod photoreceptor disks. *Biophys. J.* **83**, 1403-1412.

Corless, J. M. and Kaplan, M. W. (1979). Structural interpretation of the birefringence gradient in retinal rod outer segments. *Biophys. J.* **26**, 543-556.

Hollingworth, S., Peet, J., Chandler, W. K. and Baylor, S. M. (2001). Calcium sparks in intact skeletal muscle fibers of the frog. *J. Gen. Physiol.* **118**, 653-678.

Janson, L. W., Ragsdale, K. and Luby-Phelps, K. (1996). Mechanism and size cutoff for steric exclusion from actin-rich cytoplasmic domains. *Biophys. J.* **71**, 1228-1234.

Kaplan, M. W., Iwata, R. T. and Sears, R. C. (1987). Lengths of immunolabeled ciliary microtubules in frog photoreceptor outer segments. *Exp. Eye Res.* **44**, 623-632.

Keminer, O. and Peters, R. (1999). Permeability of single nuclear pores. *Biophys. J.* **77**, 217-228.

Lee, S. J., Xu, H., Kang, L. W., Amzel, L. M. and Montell, C. (2003). Light

adaptation through phosphoinositide-regulated translocation of Drosophila visual arrestin. *Neuron* **39**, 121-132.

Luby-Phelps, K. (2000). Cytoarchitecture and physical properties of cytoplasm, volume, viscosity, diffusion, intracellular surface area. *Int. Rev. Cytol.* **192**, 189-221.

Mangini, N. J. and Pepperberg, D. R. (1988). Immunolocalization of 48K in rod photoreceptors. Light and ATP increase OS labeling. *Invest. Ophthalmol. Vis. Sci.* **29**, 1221-1234.

Mangini, N. J., Garner, G. L., Okajima, T. I., Donoso, L. A. and Pepperberg, D. R. (1994). Effect of hydroxylamine on the subcellular distribution of arrestin (S-antigen) in rod photoreceptors. *Vis. Neurosci.* **11**, 561-568.

Mani, S. S., Besharse, J. C. and Knox, B. E. (1999). Immediate upstream sequence of arrestin directs rod-specific expression in Xenopus. *J. Biol. Chem.* **274**, 15590-15597.

Mani, S. S., Batni, S., Whitaker, L., Chen, S., Engbretson, G. and Knox, B. E. (2001). Xenopus rhodopsin promoter. Identification of immediate upstream sequences necessary for high level, rod-specific transcription. *J. Biol. Chem.* **276**, 36557-36565.

Matsumoto, B. and Besharse, J. C. (1985). Light and temperature modulated staining of the rod outer segment distal tips with Lucifer yellow. *Invest. Ophthalmol. Vis. Sci*. **26**, 628-635.

Matsumoto, B., Defoe, D. M. and Besharse, J. C. (1987). Membrane turnover in rod photoreceptors, ensheathment and phagocytosis of outer segment distal tips by pseudopodia of the retinal pigment epithelium. *Proc. R. Soc. London B Biol. Sci*. **230**, 339-354.

Mendez, A., Lem, J., Simon, M. and Chen, J. (2003). Light-dependent translocation of arrestin in the absence of rhodopsin phosphorylation and transducin signaling. *J. Neurosci*. **23**, 3124-3129.

Moritz, O. L., Tam, B. M., Knox, B. E. and Papermaster, D. S. (1999). Fluorescent photoreceptors of transgenic Xenopus laevis imaged in vivo by two microscopy techniques. *Invest. Ophthalmol. Vis. Sci*. **40**, 3276-3280.

Olson, A. and Pugh, E. N., Jr (1993). Diffusion coefficient of cyclic GMP in salamander rod outer segments estimated with two fluorescent probes. *Biophys. J.* **65**, 1335-1352.

Pazour, G. J., Baker, S. A., Deane, J. A., Cole, D. G., Dickert, B. L., Rosenbaum, J. L., Witman, G. B. and Besharse, J. C. (2002). The intraflagellar transport protein, IFT88, is essential for vertebrate photoreceptor assembly and maintenance. *J. Cell Biol.* **157**, 103-113.

Peterson, J. J., Tam, B. M., Moritz, O. L., Shelamer, C. L., Dugger, D. R., McDowell, J. H., Hargrave, P. A., Papermaster, D. S. and Smith, W. C. (2003). Arrestin migrates in photoreceptors in response to light, a study of arrestin localization using an arrestin-GFP fusion protein in transgenic frogs. *Exp. Eye Res.* **7**, 553-563.

Philp, N. J., Chang, W. and Long, K. (1987). Light-stimulated protein movement in rod photoreceptor cells of the rat retina. *FEBS Lett.* **225**, 127-132.

Pulvermuller, A., Giessl, A., Heck, M., Wottrich, R., Schmitt, A., Ernst, O. P., Choe, H. W., Hofmann, K. P. and Wolfrum, U. (2002). Calcium-dependent assembly of centrin-G-protein complex in photoreceptor cells. *Mol. Cell. Biol.* **22**, 2194-2203.

Roof, D. J. and Heth, C. A. (1988). Expression of transducin in retinal rod photoreceptor outer segments. *Science* **241**, 845-847.

Schwartz, S., Cain, J. E., Dratz, E. A. and Blasie, J. K. (1975). An analysis of lamellar X-ray diffraction from disordered membrane multilayers with application to data from retinal rod outer segments. *Biophys. J.* **15**, 1201-1233.

Tsien, R. Y. (1998). The green fluorescent protein. *Annu. Rev. Biochem*. **67**, 509-544.

Verkhusha, V. V., Kuznetsova, I. M., Stepanenko, O. V., Zaraisky, A. G., Shavlovsky, M. M., Turoverov, K. K. and Uversky, V. N. (2003). High stability of Discosoma DsRed as compared to Aequorea EGFP. *Biochemistry* **42**, 7879-7884.

Whelan, J. P. and McGinnis, J. F. (1988). Light-dependent subcellular movement of photoreceptor proteins. *J. Neurosci. Res.* **20**, 263-270.

Wilden, U., Hall, S. W. and Kuhn, H. (1986). Phosphodiesterase activation by photoexcited rhodopsin is quenched when rhodopsin is phosphorylated and binds the intrinsic 48-kDa protein of rod outer segments. *Proc. Natl. Acad. Sci. USA* **83**, 1174-1178.

Worthington, C. R. (1974). Structure of photoreceptor membranes. *Ann. Rev. Biophys. Bioeng.* **3**, 53-80.

Xu, J., Dodd, R. L., Makino, C. L., Simon, M. I., Baylor, D. A. and Chen, J. (1997). Prolonged photoresponses in transgenic mouse rods lacking arrestin. *Nature* **389**, 505-509.

Yeager, M. J. (1976). Neutron diffraction analysis of the structure of retinal photoreceptor membranes and rhodopsin. *Brookhaven Symp. Biol.* **27**, III3-III36.

ONLINE SUPPLEMENTARY MATERIALS

Materials and Methods

1. Description of the Confocal Laser Scanning Microscope

The excitation path of the CLSM consists of an Argon-ion laser (532-25A; Melles-Griot, Irvine, CA), followed by a 2 log unit neutral density wedge and absorbing filters, a 488 nm interference filter (D488/10X; Chroma Technology Corp., Brattleboro, VT), a 3X Galilean beam expander, a Nikon CFI_{60} 20X eyepiece, a long-pass (497 nm) dichroic mirror (497DCLP; Chroma Technology Corp., Brattleboro, VT), a scan mirror (6800HP & 65880F; Cambridge Technology, Inc., Cambridge, MA), and a relay lens mounted on a motorized Newport actuator (850G-HS; Newport Corp., Irvine, CA). The excitation beam is reflected by the dichroic mirror to the scan mirror, which is located at a telecentric plane conjugate to the image plane of the objective. The beam continues from the scan mirror through the eyepiece and relay lenses into the epi-fluorescence port of the TE300. Inside the TE300, the beam fills the back aperture of the objective lens with uniform, parallel 488 nm light, which is focused to a diffraction-limited spot (Airy disk) by the objective.

Fluorescent light collected by the objective lens retraces its way through the excitation path to the dichroic mirror, where it is transmitted through a 500 nm longpass, cut-on emission filter (HQ500LP; Chroma Technology Corp., Brattleboro, VT) onto a pin-hole aperture (NT53-907; if Edmund Optics Inc., Barrington, NJ) that restricts transmission to ~80% of the central maximum of the emitted light's diffraction pattern. Light passing through the aperture is divided equally by a beam splitter (05BC17MB.1; Newport Corp., Irvine, CA) and focused with two 10X objective lenses onto the active

areas of two avalanche photodiodes (SPCM-AQR-12; PerkinElmer Optoelectronics, Quebec, Canada). Pulsed TTL output from each photodiode is summed by a pair of counting modules over a programmable sampling period and converted into an analogue voltage. This voltage is converted into a 12 bit digital signal by a D to A converter unit (IDA12500, INDEC Systems Inc., Mountain View, CA) which transmits the sampled data to a PC. The PC, running customized software written in C++ (Hollingsworth paper), both records the digital signal and synchronizes data collection.

Scanning of the confocal spot in the x dimension is effected by the scan mirror, in y by vertical movement of the relay lens under control of a micropositioner (850G-HS; Newport Corp.), and in z by a generic stepping motor attached to the fine focus control of the microscope. The *y* and *z* scanning are controlled by a programmable system (ESP300-11N11N; Newport Corp., Irvine, CA), slaved and synchronized to the PC running the master-control program.

2. CLSM 3D Point-spread Function

We determined the spatial resolution of the CLSM by scanning a dilute suspension of 0.1 μm diameter fluorescent microspheres (Cat. #17l50, Polysciences, Warrngton, PA) embedded in agar (Supplementary Material, Fig. 1). The PSF distribution in the *x-y* plane (Fig. 1S-A) and that in *z* (Fig. 1S-B) were very close to those expected from diffraction optics theory (Born & Wolf, 1975, p. 440), being well described by a Gaussian function with σ = 0.13 μm and 0.26 μm, respectively, and having an overall "volume" for 90% total power of ~ 0.01 μm^3. The parameters for scanning the microspheres were as follows: *x-y* field size, 100 μm × 100 μm at 0.4 μm per pixel; *z*-step, 0.5 μm, and pixel collection time of 24 μs. The same scanning

parameters (with the exception of the z-step) were used in all the experiments reported here unless otherwise noted. In all experiments we used #1 coverslips (Cat. #12548A, Fisher Scientific) whose thickness (measured with a digital micrometer) was reliably 150 -155 μm, allowing application of an appropriate coverslip collar correction to the 60X water immersion objective.

3. Determination of EGFP concentrations from fluorescence

The relationship between fluorescence intensity and EGFP concentration, [*EGFP*], was determined by scanning a 20 μl chamber loaded with solutions of recombinant protein (Cat. #8365-1 Clontech, Palo Alto, CA) whose concentration had been determined with a recording spectrophotometer (λ20 UV/Vis, Perkin-Elmer), using published spectra and an extinction coefficient ε_{max} = 55,000 cm^2 $mmol^{-1}$ at 488 nm (Fig. 2S, A, insert; Tsien, 1998). This relationship between the excitation intensity *I*, [*EGFP*] and measured fluorescence *F* can be described as a bilinear function of the two independent variables:

$$\begin{aligned} F &= K\, I\, [EGFP] \\ &= K\, I_{max} 10^{-D}\, [EGFP] \end{aligned} \qquad (1)$$

where *I* is excitation intensity, I_{max} is the maximum intensity, *D* is the density of any absorbing filters in the excitation beam, and *K* a system constant. This relationship was found to describe the fluorescence intensity over a wide range of concentrations (Fig. 2S, A); the only practical limitation was that the output intensity at the avalanched photodiodes had to be kept below saturation, which began to set in at 20 counts μs^{-1}. This was readily achieved by decreasing the excitation intensity with interposed density filters (*D* in eqn 1).

Equation (1) was inverted in relation (1) to estimate [*EGFP*] in living cells: thus, in the volume element (voxel) at position (*x, y, z*)

$$[EGFP](x, y, z) \quad = \quad F(x, y, z) / (K\, I_{\max} 10^{-D}) \,. \qquad (2)$$

The application of the eqn (2) is illustrated in Fig. 2S, B. Potential artifacts that could be attendant on the depth of the scanning in the chamber were ruled out by scanning solutions of recombinant protein in various refractive index solutions. The

4. Transgenic Xenopus

Transgenic *Xenopus* were produced using restriction enzyme mediated integrated (REMI) as described previously (Knox et al., 1998). pXOP-EGFP (-503/+41) or pXOP (-503/+41) XAR-GFP was linearized using *X. 3*

*o*I and purified using a purification kit (Novagen) with a final elution of purified product in water. The concentration of the digested plasmid was determined using a Beckman UV-Vis spectrophotometer. The cytoplasmic phase of an interphase egg extract was added to the REMI reaction mix (containing the linearized plasmid/sperm nuclei/*Xho*I), which allows for partial decondensation and incorporation of the transgene into sperm chromatin. The REMI reaction was injected (at a flow rate of one nucleus per injection) into the animal poles of freshly collected and cysteine-dejellied eggs. Embryos undergoing normal cleavage were selected and transferred to a separate dish and cultured in 0.1X MMR at 18-20^{o}C. Transgenic animals were identified 4 days post injection by examining GFP expression, which appears to be restricted to the eye. Transgene positive and sibling controls from the same batch of injections were grown further and presence of the transgene was verified using PCR of genomic DNA from tail snips (tadpoles) or web clippings (juveniles).

5. Cloned CHO Cells Expressing EGFP

The plasmid used was produced by cloning the coding sequence for the enzymatically inactive G1651A mutant version of *LacZ* (Igoucheva et al., 1999) into the multiple cloning site of the pIRES2-EGFP plasmid (Clontech, Palo Alto, CA). The resulting plasmid (pDP3) expresses a bicistronic transcript of G1651A-*LacZ* followed by *EGFP*, under the control of the CMV promoter. To produce stably expressing cells, 10 μg of linearized pDP3 plasmid in Optimem (Invitrogen, Carlsbad, CA) was transfected into 2.5×10^5 CHO-K1 cells (ATCC, Manassas, VA) using 20 μg Lipofectamine (Invitogen), according to the manufacturer's instructions. The transfection medium was left in place for 16 hrs, and then replaced with F12K nutrient mixture (ATCC) plus 10% FCS (Hyclone, Logan, UT). Selection with G418 (Invitrogen) was initiated 36 hrs after the transfection. G418-resistant cells were then subjected to fluorescence-activated cell sorting, and the population of cells with fluorescence of exceeding 100-fold that of controls was collected. These fluorescent pDP3-CHO cells were then expanded and used for all subsequent experiments. We emphasize that the cells do not represent a true clonal line, and were expected to vary in expression level. This variation allowed us to examine the performance of the system and dependence of the estimate of cytoplasmic volume on expression level (Fig. 1). For control, a line of CHO cells (g1651a) not expressing EGFP, but also expressing enzymatically inactive *LacZ* were used. All cells were grown on F12K (ATTC) and 10% PBS. Cells at confluence were passed from the growth medium with trypsin immediately before an experiment, and their solution number density determined with standard cell-counting methods. Aliquots containing 1×10^6 cells were collected, centrifuged at 1200 RPM for 5 min at 4 ^{o}C, and the pellets

collected for Western blotting or lysate fluorimetry.

6. Description of arrestin-GFP fusion construct

To create a *Xenopus* rod arrestin-GFP fusion, a *Xma* I- *Nco* I fragment containing amino acids 17-396 of the coding region and 223 nts of the 3UTR of rod arrestin (accession number U41623) was cloned directionally into pEGFP(-) vector (Knox *et al.*, 1998) at the *Xma* I- *Not* I sites using a *Nco* I-*Not* I linker. The GFP coding sequence was amplified using gene specific primers with the 5' primer containing the first two amino acids of rod arrestin followed by a *Sal* I site and the start of the GFP coding sequence. The 3' primer contained amino acids 12-17 of arrestin and the *Xma* I site for directional cloning. Amino acids 3-4 of rod arrestin (glycine and glutamic acid) were substituted by valine and aspartic acid (conserved substitutions present in the GFP coding sequence). The resulting arrestin GFP fusion protein contains a replacement of amino acids 3-11 of rod arrestin with GFP. The rest of the fusion protein contains amino acids 12-396 of rod arrestin. This construct preserves conserved amino acids 12-16 (bovine numbering) that have been suggested to have a structural role in recognition of the light-activated form of rhodopsin (Vishnivetskiy et al., 1999). The fusion protein coding region was placed under the control of the *Xenopus* rhodopsin promoter (-503/+41) which has been shown to direct high level, rod-specific expression of reporter genes (Mani et al., 2001).

```
                1    3        11  12
                .    .        .   .
Xenopus     MS --GEKKS-RHVM   YKKT
Bos         MK --ANKPAPNHVI   FKKI
Ambymst     MS TKMSKAASRHVI   FKKT
Oryzias     MT ---GKKASRHVI   FKKT
Rana        MS --GDKKS-RSVI   YKKT
Fusion      MS --VDVSKGEELF...YKKT
```

N-terminal sequences of *Xenopus* (AAB88584), *Bovine* (P08168), *salamander* (AF203327), *Medaka* (AB029392) and *Rana pipiens* (U30269) rod arrestins and the arrestin-EGFP fusion protein used in this study. The underlined residues (and ...) are EGFP, bold residues are conserved in all proteins and dashes represent gaps. The numbering is for *Xenopus* arrestin. Alignment created using MegaAlign-ClustalW method (DNAStar 5.06).

7. Image Segmentation and Quantitative Analysis of Confocal Data from CHO Cells

A user-driven interface was created with the Matlab programming language (Mathworks, Natick, MA) for the segmentation of CLSM data from CHO cells. Three dimensional stacks of data were visualized in *x-y* planes to ascertain the approximate plane where each cell appeared widest, at plane taken to represent the cell's "equator" with respect to the image coordinates. A polygonal region was then drawn around the border of each cell at the plane of hemi-section, defining a region of interest (ROI). The corresponding ROIs were then selected from all the *x-y* planes in the three dimensional data stack, defining a 3D-ROI that completely circumscribed the data of the cell. The voxels comprising the cell were then segmented from the background in the3D-ROI based on automated thresholding using Otsu's method (Otsu, 1979).

The voxels comprising the data of each segmented cell were stored in a three dimensional matrix and subjected to further analyses. The envelope volume, V_{env}, of each cell was determined in two ways. First, V_{env} was calculated with the formula for the

volume of a sphere, based on the assumption that CHO cells passed with trypsin are spherical (see Fig. 1). Three radii were determined by measuring the distance between the central voxel of each cell (determined as the center of mass) and the maximal extent of the cell's threshold boundary in each dimension. A second estimate of V_{env} was derived by summing the volume of all of the detected voxels for each cell (for CHO cells scanned with the CLSM, each voxel measured $0.4 \times 0.4 \times 1.0$ μm). The mean fluorescence in each cell was determined by summing the intensity (counts/μs) of all voxels and dividing by the total number of voxels comprising the cell. Finally, the quantity of EGFP in each voxel was estimated by converting the intensity of each voxel into the concentration of EGFP with Eq. 2, and multiplying by the voxel volume. The total mass of EGFP in each cell was then obtained by summing over all the voxels defining the cell.

8. Image Segmentation and Quantitative Analysis of Confocal Data from Rod Cells

A method of image segmentation similar to that used for CHO CLSM data was also employed for rod data. However, the complex morphology of the rods, along with their close apposition to each other in the tissue samples (*cf*. Fig. 1), required a more complicated approach, and a special graphical user interface was developed for the purpose. Three-dimensional (3D) "stacks" of CLSM data were visualized plane by plane in order to interactively define an initial 3D-ROI comprising the rod of interest and its immediate neighbors. At the *x*-*y* plane where the rod's outer segment was most clearly visualized, two points were selected at the tip and base of the outer segment, defining the orientation of the outer segment relative to the *x*-axis. The entire 3D-ROI comprising the rod was then rotated to orient the rod outer segment data parallel to the *x*-axis (see Fig.

4A). The pixels representing the rod were then manually "cut out" from each *x*-*y* plane by drawing an *n*-degree polygon (with *n* arbitrarily large) that included the rod of interest, and excluded neighboring cells. The 3D volume defined by the inclusion regions of the polygons in all the *x*-*y* planes was then extracted from the rotated 3D- ROI and subjected to an automated threshold algorithm (Otsu, 1979). All voxels greater than or equal to the threshold were stored as the final 3D-ROI of the rod. The 3D-ROI was further divided into its respective inner and outer segments (IS and OS). The V_{env} of the IS and OS of each cell was then determined by tallying their respective voxels and multiplying by the voxel volume (measuring $0.4 \times 0.4 \times 0.5$ μm). The total fluorescence and estimation of the concentration of EGFP were determined by a method identical to those used in the analysis of the CHO cell data.

An additional feature of rod cell analysis involved deriving a spline, measuring 1.6 μm in the *x*- and *y*- dimensions and 1 μm in the z dimension, along the central "core" of each cell's 3D-ROI. To effect this, first, an averaged 2D- representation, collected from a region 1 μm thick in the z dimension, was created for each rod comprising the *x*-*y* planes where the voxels of highest intensity were located. The spline was then generated using an automated routine that averaged pixels from the center of mass of the rod in the 2D representation (main text, Fig. 4).

9. Three-dimensional representations of the CLSM data

We generated 3D representations of z-stacks of CLSM scans of living cells or frozen sections with Volview™ software (Kitware, Inc., Clifton Park, NY). With the "3D cookie cutter" individual cells could thus be visualized from various angles and perspectives, and selective fractions of their EGFP fluorescence intensity distributions

depicted with color coding. Images in Figs. 4A, 6B, 7A, 7D, 8A, 7D were generated in this way. Full 3D "avi's" of the images in Fig. 6B, 7D, 8D are provided, so that the reader may inspect some of the detail. For the avi corresponding to Fig. 3B, a linear gradient was used to display the lower 50 of the fluorescence scale, to enhance visibility of weakly expressing cells. For Figs. 6B and 7D, the lowest 5% of the intensities are shown in red (highlighting the cell boundary) and the upper 5% in green (illustrating the densest concentrations of EGFP and Arr-EGFP). For Fig. 8D, the leftmost panel was generated with a linear gradient that shows only the top 85% of the intensities; this serves to render the cell boundary more transparent, while the adjacent panels show the lowermost 5% in red, and the upper 10% in green.

SUPPLEMENTARY FIGURES AND CAPTIONS

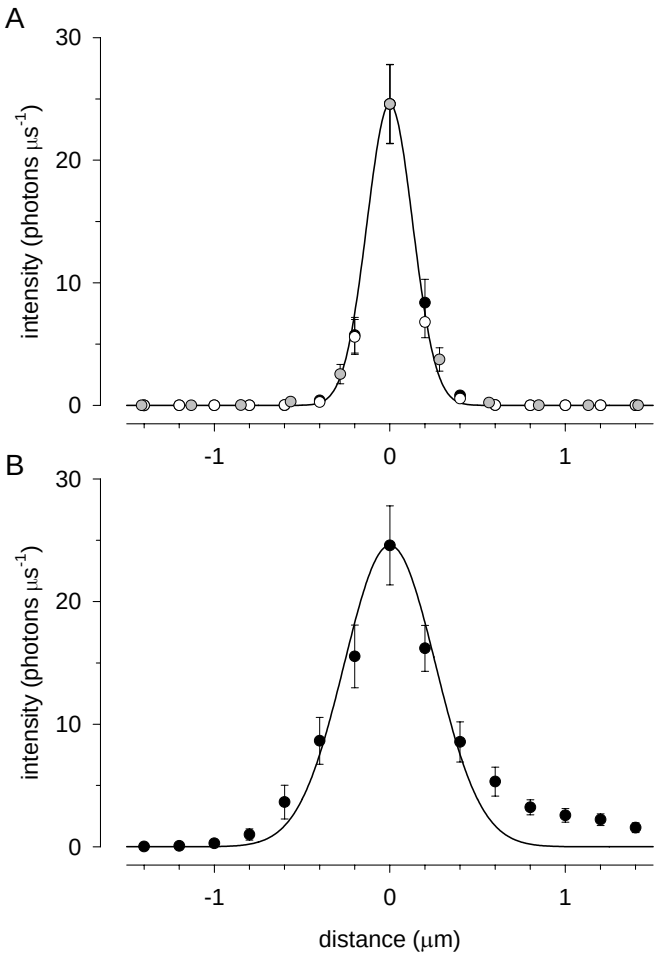

Fig. 1S. Measurement of the point-spread function of the CLSM. **A.** Averaged scans of 25 0.1 μm diameter fluorescent microspheres at the z-axis level of maximum fluorescence. Symbols represent fluorescence intensity along the pixels of the x-axis of the scan (•), along the y-axis (o), and along the diagonals, averaged (•). Error bars are 95% confidence intervals. The smooth curve through the data is a Gaussian with standard deviation $\sigma = 0.13$ μm. **B.** Data from the same scans as in panel A, but taken along the z-axis, with the positive direction corresponding to greater depth into the

chamber. The curve is a Gaussian with $\sigma = 0.26$ μm.

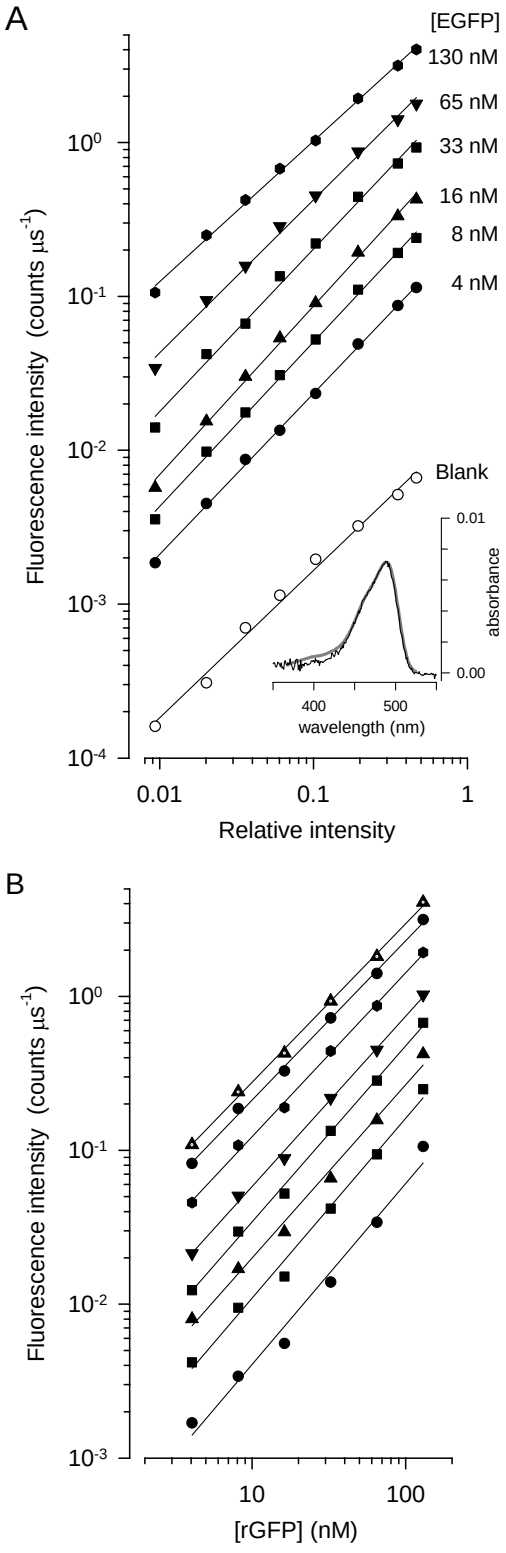

Fig. 2S. Dependence of the fluorescence intensity on the concentration of EGFP. **A.**

Each set of symbols plots for a specific concentration of EGFP the measured fluorescence as a function of the scanning beam intensity, varied by means of a neutral density wedge (EGFP concentrations are indicated by the labels adjacent to the curves. The inset shows a spectrophotometric scan (thinner black trace) of the solution with highest EGFP concentration employed, fitted with the spectrum (thicker gray trace) published by Clontech; assuming an extinction coefficient ε_{max} = 55,000 cm^2 $mmol^{-1}$ (Tsien, 1998), the derived concentration is 130 nM. The line drawn through each set of points was obtained with a least-squares regression fitting procedure: their slopes (fitted in linear coordinates, starting with the set of points for the "blank" and proceeding to the set for 130 nM) are 0.96, 1.05, 1.07, 1.10, 1.06, 0.99, 0.91. **B.** The data of panel A have been replotted as a function of the concentration of EGFP, after subtraction of the "blank". The least-squares regression lines (starting with the lowest set of points and proceeding to the uppermost) have slopes 1.17, 1.17, 1.12, 1.14, 1.05, 1.06. 1.03, 1.03.

References

Born M., and Wolf E. 1975. Principles of Optics. Pergamon Press, New York. (cf. Section 8.8.2).

Knox, B., Schlueter, C., Sanger, B., Green, C. and Besharse, J. 1998. Transgene expression in *Xenopus* rods. *FEBS Lett.* **423**(2):117-121.

Igoucheva *et al*. 1999. A sequence-specific gene correction by an RNA-DNA oligonucleotide in mammalian cells characterized by transfection and nuclear extract using a lacZ shuttle system. *Gene Therapy* **6**(12): 1960-1971.

Mani, S. S., Besharse, J. and Knox, B. 1999. Immediate upstream sequence of arrestin directs rod-specific expression in *Xenopus*. *J. Biol. Chem.* **274**: 15590-15597.

Mani SS, Batni S, Whitaker L *et al*. 2001. *Xenopus* rhodopsin promoter. Identification of immediate upstream sequences necessary for high level, rod-specific transcription. *J. Biol. Chem*. **276**(39): 36557-36565.

Otsu, N. 1979. A threshold selection method from gray-level histograms. *IEEE Transactions on Systems, Man, and Cybernetics*. 9(1): 62-66.

Tsien, R.Y. 1998. The green fluorescent protein. *Annu. Rev. Biochem*. **67**: 509-544.

Vishnivetskiy S. A., Paz C. L., Schubert C., Hirsch J. A. , Sigler P. B., Gurevich V. V. 1999. *J. Biol. Chem.* **274**, 11451-11454.